A Low-Complexity Optimal Switching Time Modulated Model Predictive Control for PMSM with Three-Level NPC Converter

Qi Wang, *Student Member, IEEE,* Haitao Yu, Chen Li, *Student Member, IEEE,* Xiaoyu Lang, *Student Member, IEEE,* Seang Shen Yeoh, Tao Yang, *Member, IEEE,* Marco Rivera, *Senior Member, IEEE,* Serhiy Bozhko, *Senior Member, IEEE,* and Patrick Wheeler, *Senior Member, IEEE*

***Abstract*—Conventional finite control set model predictive control (FCS-MPC) presents high computational burden especially in three-level neutral point clamped (NPC) converters. This paper proposes a low-complexity optimal switching time modulated model predictive control (OST-M2PC) method for three-level NPC converter. In the proposed OST-M2PC method, the optimal switching time is calculated using a cost function. Compared to conventional FCS-MPC, the proposed OST-M2PC method has a fixed switching frequency as well as better power quality. The proposed OST-M2PC can operate at a 20kHz sampling frequency, reducing the computational burden of the processor. Simulation and experimental results validate the operation of the proposed method.**

***Index Terms*—Finite control set model predictive control (FCS-MPC), modulated model predictive control (M2PC), permanent magnet synchronous motor (PMSM), optimal switching time modulated model predictive control (OST-M2PC).**

I. Introduction

Permanent magnet synchronous motors (PMSMs) have been widely used in fields of high-performance servo systems and other industrial applications, due to high efficiency, high power density and other advantages [1]. Generally, a fast current response is required to guarantee high dynamic performance of PMSM drive system. The PI control method is often adopted as the current control method for PMSMs [2]. However, a PI controller is a linear controller with a confliction between system stability and dynamic performance. Some nonlinear methods such as fuzzy control [3], neural network control, sliding mode control [4] and predictive control [5] are gradually being introduced as processor performance improves. Finite control set model predictive control (FCS-MPC) for a three-level neutral point clamped (NPC) converter is firstly introduced by Jose Rodriguez *et all* [6]. A discrete time model is used to predict controller current in next sampling period, and all switching actions are evaluated with a cost function. The switching action which minimizes the cost function is selected to be applied to the control system. FCS-MPC generates a switching signal directly, without modulation. FCS-MPC has been widely implemented by the academic and industrial community [7]–[10]. However, FCS-MPC needs high sampling frequency to ensure good control performance, because of variable switching frequency, requiring an often excessive computational time [11].

Several solutions have been proposed to overcome these drawbacks. For example, in [8], Reza Nasiri *et all* improved the traditional FCS-MPC for a multilevel converter by solving the diophantine equations so that proposed method can run on single core processor. Although this proposed method save most compuational time of processor, it still has variable switching frequency. In [12], the duty cycle model predictive control method with a PWM rectifier is proposed. In this method, one nonzero vector is selected and the duty cycle of zero vector is analytically derived. These two vectors are implemented during each sampling period, achieving better steady-state performance. However, only the length of the resultant vector is variable and direction is still fixed. Therefore, it also has an adjustable switching frequency as well as a high current total harmonic distortion (THD). Xiong *et all* proposed a constant switching frequency MPC method for a five-phase PMSM, which can acquire virtual voltage vectors and their duty ratios by a dead-beat based method directly [1]. However, optimal virtual voltage vectors are selected in two orthogonal subspaces and voltage sequences need to be rearranged by carrier-based pulsewidth modulation (CBPWM), therefore, this proposed algorithm is still complicated. It can be seen from the experiment results that this method can only operate at 10*kHz* sampling switching using TMS320F28335. To suppress the current ripples of FCS-MPC, a fixed switching method called modulated model predictive control (M2PC) was first proposed by Tarisciotti *et al*. [13]. This method was applied to a seven-level cascaded H-bridge converter [14] and an indirect matrix converter [15]. In [16], an M2PC is studied for two-level

Manuscript received April 28, 2020; revised June 22, 2020; accepted July 21, 2020. This work was supported by the National Natural Science Foundation of China under Projects 41576096, the Clean Sky 2 Joint Undertaking under Grant 807081 and the Fondecyt Regular Project 1160690. (*Corresponding author: Haitao Yu.)*

Q. Wang, and H.T. Yu are with School of Electrical Engineering, Southeast University, Nanjing, 210096, China (e-mail: qwang.cn@outlook.com; htyu@seu.edu.cn).

C. Li, X.Y. Lang, S.S. Yeoh, T. Yang, S. Bozhko, and P. Wheeler are with the Power Electronics, Machines and Control Group, The University of Nottingham, Nottingham NG7 2RD, U.K (e-mail: chen.li@nottingham.ac.uk; Xiaoyu.Lang@nottingham.ac.uk;Seang.Yeoh@nottingham.ac.uk; tao.yang@nottingham.ac.uk;serhiy.bozhko@nottingham.ac.uk;pat.wheeler@nottingham.ac.uk).

M. Rivera is with the Department of Electrical Engineering, Universidad de Talca, Curico, 3341717,Chile (e-mail: marcoriv@utalca.cl).

voltage source inverter and compared with the traditional FCS-MPC. M2PC has a higher average switching frequency than conventional FCS-MPC at the same sampling frequency as well as better power quality and lower THD. However, this algorithm needs to calculate the two adjacent vectors of all sectors in each sampling period. For a two-level voltage source inverter, the number of calculations is 12, which causes a large computational burden. Meanwhile, duty ratios for the synthesized vectors are evaluated by a cost function, which undermines the accuracy of synthesized vector. M2PC for a three-level NPC converter was first proposed by *Rivera* et al. [17]. The experimental results of two types of the M2PC methods for a three-level NPC converter were presented by *Donoso* et al. using a DSPACE-FPGA control platform [18]. More computation time is required for a three-level NPC converter, because for M2PC, it needs to calculate a total of 27 vectors in each sampling period.

In [11], a FCS-MPC method based on predictive voltage control for a three-level NPC converter was proposed to reduce the computational time of the processor. This proposed method has two steps: firstly, the predictive voltage calculation instead of current prediction; Secondly, a reduced number of cost function calculations. In this way, the computation burden of processor is reduced while maintaining the same control performance as conventional FCS-MPC. However, this method is essentially the same as conventional FCS-MPC, which has a variable switching frequency as well as a larger current ripple than M2PC [17]. In [19], an optimal switching sequence model predictive control for a vienna converter was proposed. The optimal duty ratios can be required by minimizing errors of current. However, the cost function is still a function of actual current and the reference current, the cost function and optimal duty ratios need to be calculated six times in each sampling period, still causing a heavy computation burden.

In order to reduce computation burden of the processor and have a fixed switching frequency to improve harmonic spectrum, a low-complexity optimal switching time modulated model predictive control (OST-M2PC) method for a three-level NPC converter is proposed in this paper. First, a hexagon sector division method is used instead of the triangle sector division method in the three-level phase plane. Small sectors can be quickly selected using the predicted voltage. Then, the dwell times of adjacent vectors in each small sector can be calculated using the cost function, which are the length of the predicted voltage vector and adjacent voltage vectors. Finally, the voltage vector of the next period is synthesized by the dwell times of adjacent vectors. The main research contents of this paper are as follows:

1) The execution time of conventional FCS-MPC is analyzed; a simplified FCS-MPC for three-level NPC converter is introduced.
2) A low-complexity OST-M2PC method is proposed and implementation of this proposed method is described in detail.
3) The execution time for different MPC methods, such as FCS-MPC, M2PC, simplified FCS-MPC and OST-M2PC are compared.
4) The harmonic spectrum of a phase current for simplified FCS-MPC, M2PC and OST-M2PC are analyzed in detail.

The remainder of this paper is organized as follows: Section II introduces the conventional FCS-MPC for PMSM using three-level NPC converter, then introduces a simplified FCS-MPC method. A low-complexity OST-M2PC is given in Section III. Comparative simulation and experimental studies of proposed OST-M2PC and simplified FCS-MPC are presented in Section IV. Finally, the conclusions are drawn in Section V.

II. Conventional Finite Control Set Model Predicitive Control Method

A. FCS-MPC for PMSM with There-level NPC Converter

The switching states (P, O, and N) for a typical three-level NPC converter can be seen in Fig. 1.

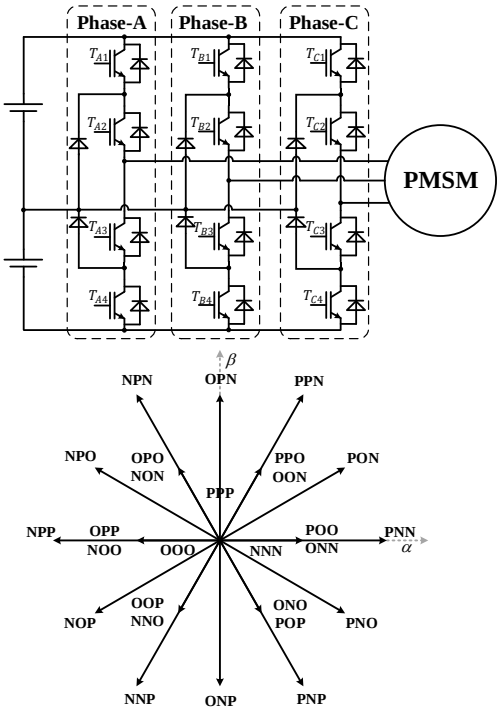

Fig. 1. The structure and vector diagram of three-level neutral-point-clamped (NPC) converter.

Assuming that magnetic circuit is not saturated and igonring hysteresis eddy current [20], [21], the *d*-*q* axis voltage model of PMSM is shown in equation (1).

$$\begin{cases} u_d = R_s i_d + L_d \dfrac{di_d}{dt} - L_q \omega_e i_q \\ u_q = R_s i_q + L_q \dfrac{di_q}{dt} + L_d \omega_e i_d + \psi \omega_e \end{cases} \tag{1}$$

L_q , L_d , and R_s are the *q*-axis inductance, the *d*-axis inductance, and the stator resistance, respectively; ω_e and ψ are the electrical speed of PMSM and the flux linkage, respectively. u_q , u_d are the *q*-axis voltage, *d*-axis voltage, respectively. Then, a discrete time predictive *d*-*q* axis currents

can be obtained, as shown in equation (2). T_s is sampling time, k is sampling interval.

$$\begin{cases} i_d^p(k+1)=\left(1-\dfrac{R_sT_s}{L_d}\right)i_d(k)+\dfrac{T_sL_q}{L_d}\omega_e i_q(k)+\dfrac{T_s}{L_d}u_d(k) \\ i_q^p(k+1)=\left(1-\dfrac{R_sT_s}{L_q}\right)i_q(k)-\dfrac{T_sL_d}{L_q}\omega_e i_d(k)-\dfrac{\psi\omega_eT_s}{L_q}+\dfrac{T_s}{L_q}u_q(k) \end{cases} \tag{2}$$

The conventional FCS-MPC takes all 27 vectors into equation (2) to calculate predictive d-q axis currents at the next sampling time, then uses the predictive d-q axis currents to calculate cost function as follows [22],

$$g=\left(i_d^*-i_d^p(k+1)\right)^2+\left(i_q^*-i_q^p(k+1)\right)^2 \tag{3}$$

The vector which can minimize the cost function is selected and used in next sampling time. Control diagram of conventional FCS-MPC control method with three-level NPC inverter is shown in Fig. 2. Only one basic vector is selected in each sample period which causes a high current total harmonic distortion (THD) as well as the torque ripple of PMSM [23], see references[17], [24] for details. Meanwhile, a total of 27 basic voltage vectors (including eight redundant voltage vectors) are available in a three-level NPC converter. All vectors need to be predicted by equation (2) and calculated by equation (3), the total calculation time of equation (2) and (3) is 54 in each sampling period, causing a heavy computational burden of processor and hard to run in a high switching frequency.

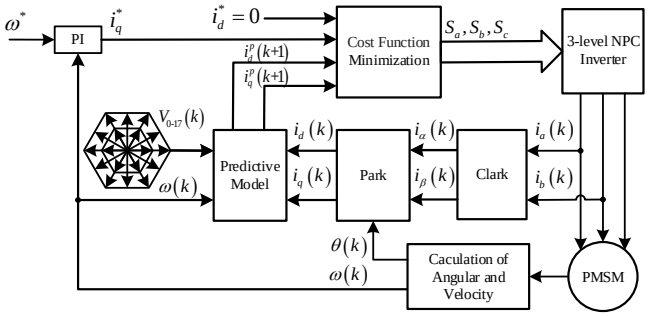

Fig. 2. Control diagram of conventional FCS-MPC control method with three-level NPC inverter.

B. Simplified Finite Control Set Model Predicitive Control Method

To implement FCS-MPC at a high switching frequency as well as reduce computing burden of the processor, a simplified finite control set model predictive control (SFCS-MPC) for a PMSM is proposed. By discretizing equation (1), the d-q axis voltages can be obtained as follows:

$$\begin{cases} u_d(k)=R_si_d+L_d\dfrac{i_d(k+1)-i_d(k)}{T_s}-L_q\omega_e i_q(k) \\ u_q(k)=R_si_q+L_q\dfrac{i_q(k+1)-i_q(k)}{T_s}+L_d\omega_e i_d(k)+\psi\omega_e \end{cases} \tag{4}$$

Substituting the reference d-q axis currents into equation (4), d-q axis predictive voltages can be shown as:

$$\begin{cases} u_d^p(k)=R_si_d+L_d\dfrac{i_d^*(k+1)-i_d(k)}{T_s}-L_q\omega_e i_q(k) \\ u_q^p(k)=R_si_q+L_q\dfrac{i_q^*(k+1)-i_q(k)}{T_s}+L_d\omega_e i_d(k)+\psi\omega_e \end{cases} \tag{5}$$

Therefore, the α-β axis voltages of predictive vector can be obtained using the inverse Park transformation [25]:

$$\begin{cases} u_\alpha^p(k)=u_d^p(k)\cos\theta-u_q^p(k)\sin\theta \\ u_\beta^p(k)=u_d^p(k)\sin\theta+u_q^p(k)\cos\theta \end{cases} \tag{6}$$

From equation (6), the origin point of selected hexagon can be obtained. θ is electrical angle of PMSM. As shown in Fig. 3, the solution of the proposed SFCS-MPC method is the same as the conventional two-level FCS-MPC in each hexagon. V^p and U_2^p are original voltage vector, new mapping voltage vector, respectively. The new mapping voltage vector in stationary axis can be calculated from Table I.

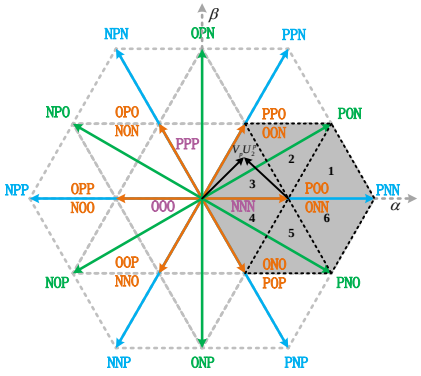

Fig. 3 The sector division method of SFCS-MPC for three-level NPC converter.

Then, the cost function can be calculated using the next equation.

$$g=\left(u_{\alpha2}^p(k)-u_\alpha^i(k)\right)^2+\left(u_{\beta2}^p(k)-u_\beta^i(k)\right)^2 \tag{7}$$

Where, $i=0,\ldots,6$. From equation (7), it can be seen that the cost function is the distance of predictive vector and basic vector. This definition of cost function is first proposed by *Xia* [11]. This proposed FSC-MPC only needs one-time prediction, sequently reduces computational burden of processor.

TABLE I
STATIONARY AXIS VOLTAGES IN EACH HEXAGON

Hexagon Sector	α -axis voltage $u_{\alpha2}^p$	β -axis voltage $u_{\beta2}^p$
1	u_α^p -V_{dc}/3	u_β^p +V_{dc}/6
2	u_α^p -V_{dc}/6	u_β^p -V_{dc}/6
3	u_α^p +V_{dc}/6	u_β^p -V_{dc}/3
4	u_α^p +V_{dc}/3	u_β^p -V_{dc}/6
5	u_α^p +V_{dc}/6	u_β^p +V_{dc}/6
6	u_α^p -V_{dc}/6	u_β^p +V_{dc}/3

III. PROPOSED OST-M2PC METHOD

To reduce the THD of a-phase current using conventional FCS-MPC, a new solution named M2PC which has a fixed switching frequency is developed [26]. In the conventional two-level M2PC method, both predictions and cost functions $g1$, $g2$ are evaluated by two adjacent vectors in each sector [16]. The total number of calculations is 12. In three-level M2PC method, the total number of calculations is 72, because there are 24 small sectors, each of which has three large voltage vectors. Details of M2PC method for three-level NPC converter can be found in [17], [18]. The conventional M2PC has a fixed switching frequency as well as better power quality than FCS-MPC. However, the number of executions of (2) and (3) in the conventional M2PC is 144 [17], which increases the computation burden of the processor. Due to limited space of this paper, please refer to references [17], [23] for details of M2PC. This paper introduces a low-complexity OST-M2PC to reduce the calculation burden. Different from the conventional M2PC, the proposed OST-M2PC adopts predictive voltages in next sampling time, as shown in equation (5). Only one-time prediction is needed (the number of executions of (5) is 1) in each sampling period and one sector is selected by predictive voltage quickly, reducing the computation time. The sector division method of this proposed technique still adopts six hexagon division, as shown in Fig. 3.

A. Sector Selection of Proposed OST-M2PC

The large hexagon sector can be selected by static coordinate predictive voltage vector. Each large hexagon sector is located in the fixed angle range by equation (8) and Table II.

$$\begin{cases} u_{\alpha}^{p} > 0 & A = 1, otherwise, A = 0 \\ \sqrt{3}u_{\alpha}^{p} + 3u_{\beta}^{p} > 0 & B = 1, otherwise, B = 0 \\ 3u_{\beta}^{p} - \sqrt{3}u_{\alpha}^{p} > 0 & C = 1, otherwise, C = 0 \\ N = 4A + 2B + C \end{cases} \tag{8}$$

TABLE II
LARGE SECTOR DIVISION OF OST-M2PC METHOD

N	0	1	3	4	6	7
Sector number	5	4	3	6	1	2

Each large sector has its own six small sectors. The new mapping voltage vector in static coordinate can be determined from Table II. The space vector diagram of three-level is converted to that of two-level by shifting origin point of each large sector, as shown in Fig. 3.

A total of six small sectors in each large sector, the selection of each small sector is same as conventional two-level space vector pulse width modulation (SVPWM) method. Taking the first large sector as an example, the predictive voltage vector in the stationary axis are $u_{\alpha 2}^{p}(k)$, $u_{\beta 2}^{p}(k)$, respectively. The small sector can be selected using equation (9) and Table III.

$$\begin{cases} u_{\beta 2}^{p} > 0 & X = 1, otherwise, X = 0 \\ \sqrt{3}u_{\alpha 2}^{p} - u_{\beta 2}^{p} > 0 & Y = 1, otherwise, Y = 0 \\ -\sqrt{3}u_{\alpha 2}^{p} - 3u_{\beta 2}^{p} > 0 & Z = 1, otherwise, Z = 0 \\ M = X + 2Y + 4Z \end{cases} \tag{9}$$

TABLE III
SMALL SECTOR DIVISION OF OST-M2PC METHOD

M	1	2	3	4	5	6
Sector number	2	6	1	4	3	5

B. Optimal Switching Time Calculation of Proposed Method for There-level NPC Converter

In the conventional M2PC method, dwell times for two adjacent voltage vectors and the zero voltage vector are calculated from a proportional relationship. The switching frequency can be fixed by modulation, but the dwell times of the adjacent voltage vectors are not optimal. To overcome this problem, this paper presents an optimal switching time calculation method which is similar to the one proposed by *Shin-Won* et al. [27]. Reference [27] uses the cost function to calculate the optimal duration ratio of the symmetrical three vector for two-level voltage source inverter. Here, through expanding this method to a three-level NPC converter, calculating the optimal switching time in the selected mapping small sector is proposed. Take first small sector of large sector for example, as shown in Fig. 4, the dwell times of two adjacent vectors and zero vector are T_1, T_2, T_0, respectively. Therefore, the resultant vector in stationary coordinate can be defined as follows:

$$\begin{cases} T_s V_{\alpha} = V_{\alpha 1} T_1 + V_{\alpha 2} T_2 + V_{\alpha 0} T_0 \\ T_s V_{\beta} = V_{\beta 1} T_1 + V_{\beta 2} T_2 + V_{\beta 0} T_0 \end{cases} \tag{10}$$

Where, $V_{\alpha 1}$, $V_{\alpha 2}$, $V_{\alpha 0}$ are the α-axis component of voltage vector V_1, V_2 and V_0. $V_{\beta 1}$, $V_{\beta 2}$, $V_{\beta 0}$ are the β-axis component of voltage vector V_1, V_2 and V_0. As shown in equation (11), the new dwell times d_1, d_2, d_0 can be obtained by normalizing dwell times T_1, T_2, T_0, respectively.

$$\begin{cases} V_{\alpha} = V_{\alpha 1} d_1 + V_{\alpha 2} d_2 + V_{\alpha 0} d_0 \\ V_{\beta} = V_{\beta 1} d_1 + V_{\beta 2} d_2 + V_{\beta 0} d_0 \\ d_0 = T_0 / T_s \\ d_1 = T_1 / T_s \\ d_2 = T_2 / T_s \end{cases} \tag{11}$$

The proposed OST-M2PC can find out the optimal dwell times of resultant voltage vectors as well as solving optimal d_1, d_2, d_0. Therefore, the cost function can be defined as follows:

$$g = \left(u_{\alpha 2}^{p} - V_{\alpha}\right)^2 + \left(u_{\beta 2}^{p} - V_{\beta}\right)^2 \tag{12}$$

$u_{\alpha 2}^{p}$ and $u_{\beta 2}^{p}$ are the predictive voltages in mapping small sector. Optimal dwell times of resultant voltage vectors can be solved using equation (13).

$$\begin{cases} \dfrac{\partial g}{\partial d_1} = \dfrac{\partial\left(\left(u_{\alpha 2}^{p} - V_{\alpha 1}\right)^2 + \left(u_{\beta 2}^{p} - V_{\beta 1}\right)^2\right)}{\partial d_1} = 0 \\ \dfrac{\partial g}{\partial d_2} = \dfrac{\partial\left(\left(u_{\alpha 2}^{p} - V_{\alpha 2}\right)^2 + \left(u_{\beta 2}^{p} - V_{\beta 2}\right)^2\right)}{\partial d_2} = 0 \end{cases} \tag{13}$$

According to the equations (11) and (13), the optimal dwell times of resultant voltage vectors can be obtained as:

$$\begin{cases} d_1 = \left(AC - BD\right) \Big/ \left(B^2 - A^2\right) \\ d_2 = \left(AD - BC\right) \Big/ \left(B^2 - A^2\right) \end{cases} \tag{14}$$

Where,

$$\begin{cases} A = {V_{\alpha 1}}^2 + {V_{\beta 1}}^2 \\ B = V_{\alpha 1} V_{\alpha 2} + V_{\beta 1} V_{\beta 2} \\ C = -u_{\alpha 2}^{p} V_{\alpha 1} - u_{\beta 2}^{p} V_{\beta 1} \\ D = -u_{\alpha 2}^{p} V_{\alpha 2} - u_{\beta 2}^{p} V_{\beta 2} \end{cases} \tag{15}$$

The proposed OST-M2PC only needs one-time prediction to find out sector, then the optimal dwell times of resultant voltage vectors can be calculated by equations (14) and (15), reducing the computational burden of processor effectively. The execution time of the proposed OST-M2PC and some conventional methods will be compared in Part IV.

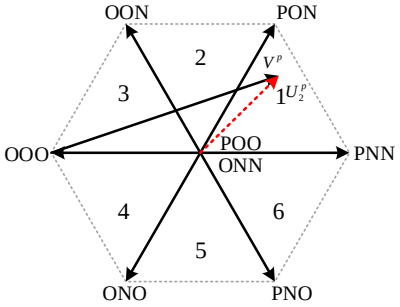

Fig. 4. The diagram of the original voltage vector and the new resultant voltage vector (sector 1).

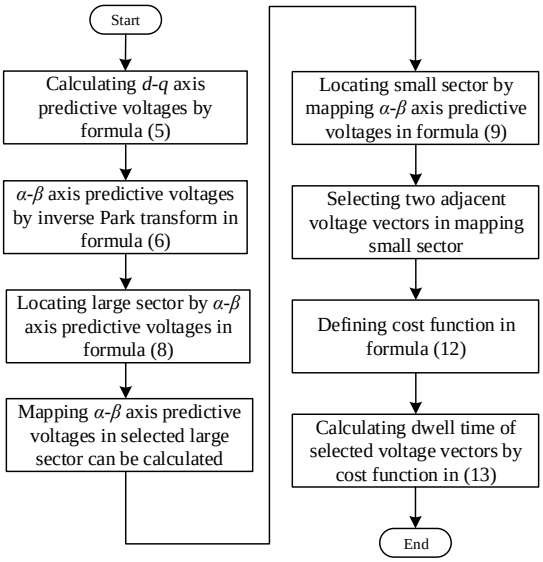

Fig. 5. The flow chart of the proposed OST-M2PC.

Fig. 5 shows the flow chart for the proposed OST-M2PC, this flow chart begins with the calculation of *d-q* axis predictive voltages of PMSM. Then, the *α-β* axis predictive voltages of PMSM can be obtained using Park transformations. The large sector can be located and the mapping *α-β* axis predictive voltages in selected large sector can be obtained in Table I. Two adjacent voltage vectors and small sector can be selected by mapping *α-β* axis predictive voltages. Finally, the cost function can be calculated with the resultant voltage vectors and predictive voltage vectors for comparison of minimal. The dwell times of the two adjacent voltage vectors can be obtained and applied.

IV. Simulation and Experimental Results

Simulation and experimental results have been used to validate the proposed OST-M2PC and SFCS-MPC in a PMSM system with a three-level NPC converter. The parameters of the PMSM are shown in Table IV. The sampling frequency of the three-level NPC converter is 20*kHz*.

TABLE IV
PARAMETER SETTING OF PMSM

Parameter	Symbol	Value
Rated Voltage	V	230 V
Stator Phase Resistance	R	1.2 Ω
Motor Inertia	J	0.0116 $kg.m^2$
Pole Pairs	P_n	3 *Pair*
Rated Torque	T_e	8.1 $N.m$
q-axis Inductance	L_q	8.379 mH
d-axis Inductance	L_d	6.17 mH
Machine mutual flux	ψ_m	0.23 Vs
Viscous damping	B	0.0015 Nms

A. Simulation Results

Figs. 6, 7 and 8 show dynamic load disturbance simulation results of the SFCS-MPC, M2PC [17] and the proposed OST-M2PC, respectively. The target speed is 1000*rpm*. An external torque load is applied to test system at t = 0.3*s*. The *q*-axis current increases quickly, showing the robustness of the control system to a load disturbance. From Fig. 6 (a)-(c), shows three phase current and *d-q* axis currents of SFCS-MPC, respectively. Fig. 7 shows responses of *d-q* axis currents and three phase current operating with M2PC. The *d-q* axis currents and a phase current of proposed OST-M2PC are shown in Fig. 8. From Figs. 6-8, the dynamic responses of these three approaches can be seen to be exactly the same. However, the M2PC has a lower current ripple than the SFCS-MPC. The proposed OST-M2PC has a lowest current ripple by calculating optimal dwell times. The waveform spectrum for these three methods at steady 1500*rpm* are shown in Figs. 9, 10 and 11, respectively.

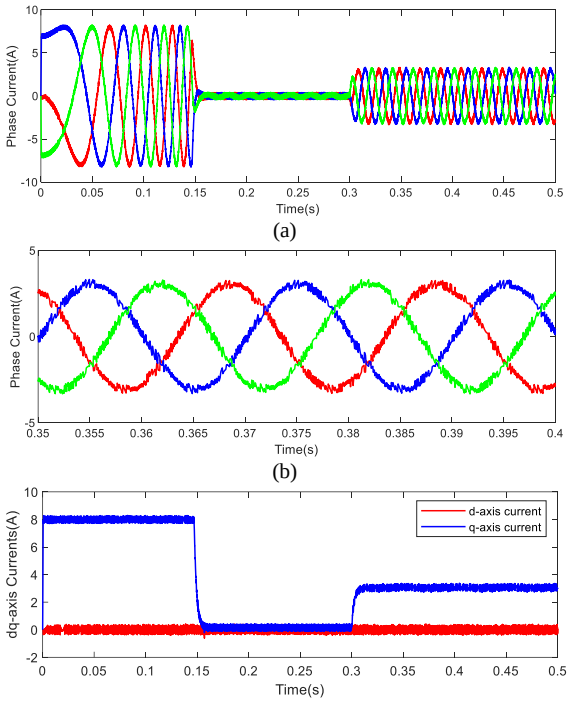

Fig. 6. Simulation results of SFCS-MPC. (a) A-phase current. (b) A-phase current(0.35*s*-0.4*s*). (c) *d*-*q* axis currents.

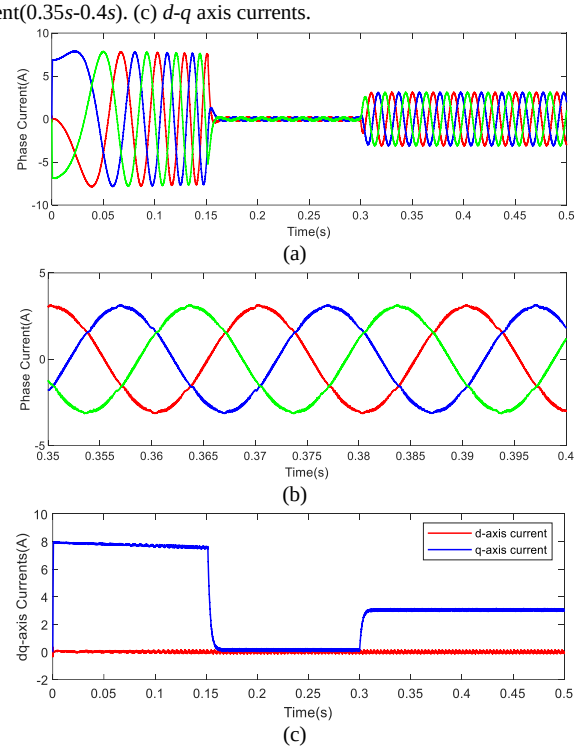

Fig. 7. Simulation results of M2PC. (a) A-phase current. (b) A-phase current(0.35*s*-0.4*s*). (c) *d*-*q* axis currents.

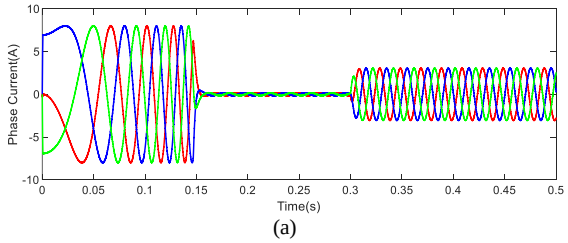

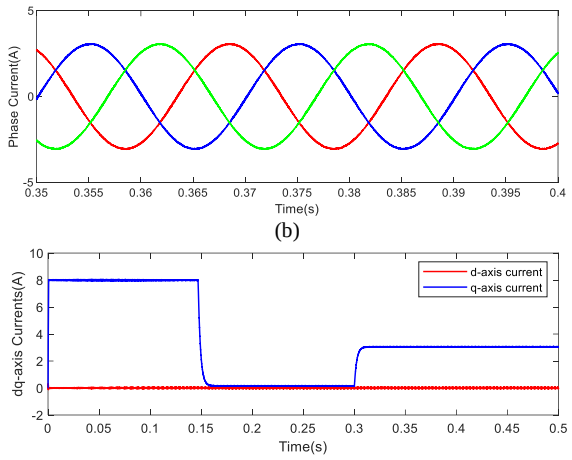

Fig. 8. Simulation results of proposed OST-M2PC. (a) A-phase current. (b) A-phase current(0.35*s*-0.4*s*). (c) *d*-*q* axis currents.

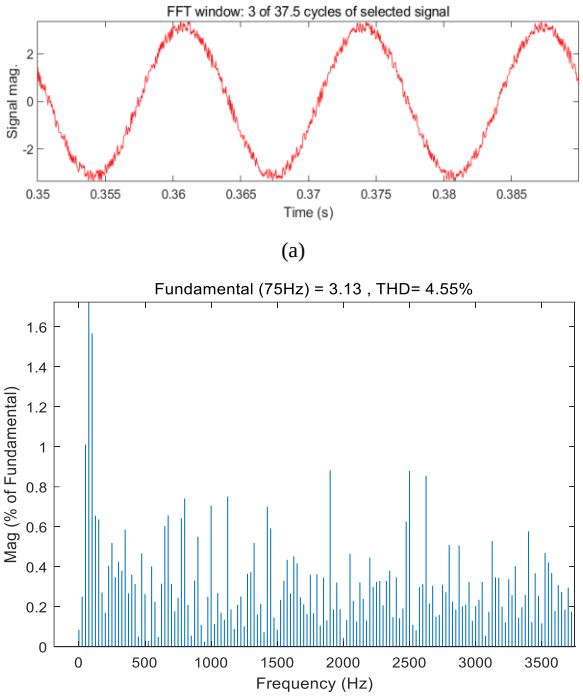

Fig. 9. The output waveform specturm for SFCS-MPC (simulation). (a) A-phase current. (b) Harmonic spectrum of A-phase current.

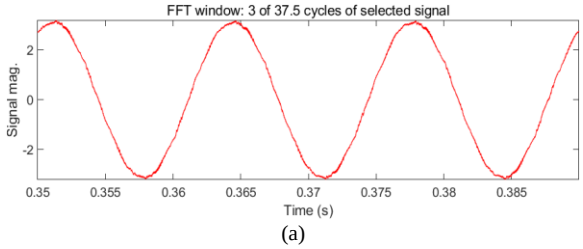

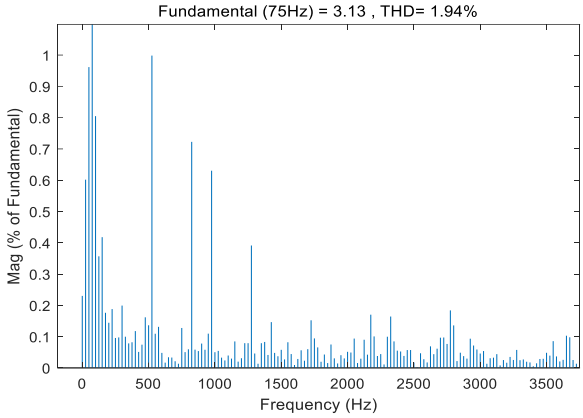

(b)

Fig. 10. The output waveform specturm for M2PC (simulation). (a) A-phase current. (b) Harmonic spectrum of A-phase current.

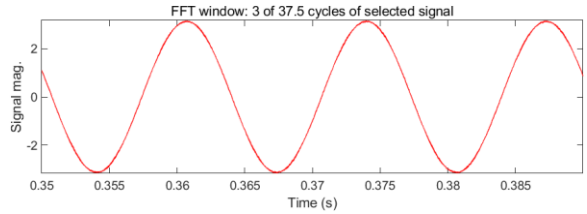

(a)

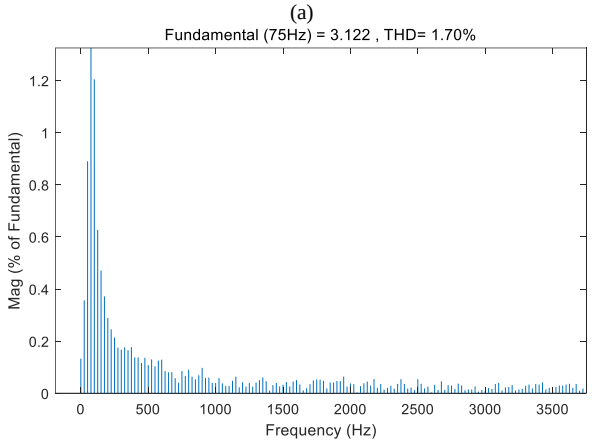

(b)

Fig. 11. The output waveform specturm for OST-M2PC (simulation). (a) A-phase current. (b) Harmonic spectrum of A-phase current.

TABLE V
THD OF A-PHASE CURRENT UNDER VARIOUS SPEED

Speed	Methods	THD
600*rpm*	SFCS-MPC	3.76%
	M2PC	3.16%
	OST-M2PC	2.45%
1000*rpm*	SFCS-MPC	4.07%
	M2PC	1.99%
	OST-M2PC	0.41%
1500*rpm*	SFCS-MPC	4.55%
	M2PC	1.94%
	OST-M2PC	1.70%

The THD of the SFCS-MPC method, M2PC method and proposed OST-M2PC method are 4.55% , 1.94% and 1.7%, respectively. The THD of a-phase current at different speeds is summarized in Table V. It can be seen that the proposed OST-M2PC has the lowest THD as well as better power quality than the other two methods.

B. Experimental Results

A prototype PMSM control system with a three-level NPC converter was built to test the proposed method. Fig. 12 shows the photograph of the experimental test rig. The PMSM (Emerson, 115UMC Series) is powered by a three-level NPC converter. A DC motor (TT Electric, LAK 2100-A) is used as a load. The main controller is a floating digital signal processor (Texas Instrument, TMS320F28335) running with a 150*MHz* clock frequency. All experimental results are from an oscilloscope with a 12-bit high-speed digital analog (DA) converter. The sampling time is 50 μs .

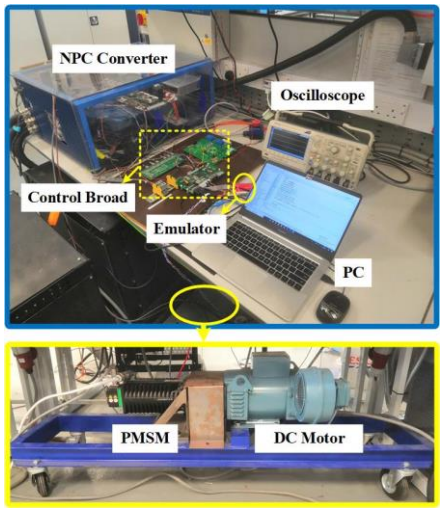

Fig. 12. Photograph of experimental test rig with three-level NPC converter.

The running time in each sample period can be seen from Fig .13. For different MPC algorithms, only the running time of step 4 is different. The running time required in TMS320F28335 by different methods in step 4 are shown in Table IV. As seen in this table, the running time of conventional FCS-MPC, MP2C [17], SFC-M2PC and OST-M2PC are obtained using CCS 6.2 (Texas Instrument Company, Code Composer Studio Integrated Development Environment) are 218 μs , 384 μs , 17.6 μs and 26.7 μs , respectively. FCS-MPC and MP2C cannot run in one sampling period (50 μs in one sampling period). Therefore, only comparison experiments for SFCS-MPC and OST-M2PC methods are implemented at 20*kHz* sampling frequency. The proposed SFCS-MPC and OST-M2PC reduce the computational burden of processor, but the OST-M2PC needs more running time than SFCS-MPC.

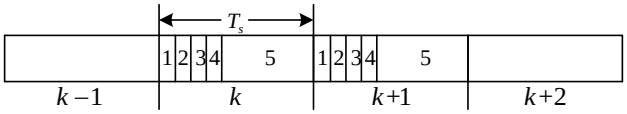

1：AD sample and angle measure
2：Coordinate transformation
3：Speed PI calculate
4：Predictive control algorithm
5：Free time

Fig. 13. Runing time required in each sample period.

TABLE IV
RUNING TIME REQUIRED IN TMS320F28335 BY DIFFERENT METHODS

Method	FCS-MPC	M2PC	SFCS-MPC	OST-M2PC
Runing time required in TMS320F28335	218 μs	384 μs	17.6 μs	26.7 μs

Figs. 14-16 show dynamic response abilities of the OST-M2PC and SFCS-MPC methods. Fig.14 shows experimental results under speed changing from 200*rpm* to 1000*rpm*. SFCS-MPC and proposed OST-M2PC have the same dynamic performance. The PMSM can achieve target speed 1000*rpm* within 200*ms*. Fig. 15 shows experimental results under speed changing from 1000*rpm* to 200*rpm*. It is clearly seen that the speed of PMSM tracks the target speed quickly and accurately. The current ripples of SFCS-MPC are much higher than proposed OST-M2PC. Fig. 16 shows experimental results under sudden load disturbance at 1000*rpm*. The proposed OST-M2PC and SFCS-MPC have same disturbance rejection potential as well as fast response ability of current loop, the speed of PMSM can recovery within 100*ms*.

Figs. 17-18 show the steady responses for the OST-M2PC and SFCS-MPC methods. The harmonic analysis of SFCS-MPC and OST-M2PC are shown in Figs. 17 and 18, respectively. It can be seen that the THD for the SFCS-MPC and OST-M2PC are 5.66% and 3.01%, respectively. The proposed OST-M2PC has lower current ripple than SFCS-MPC.

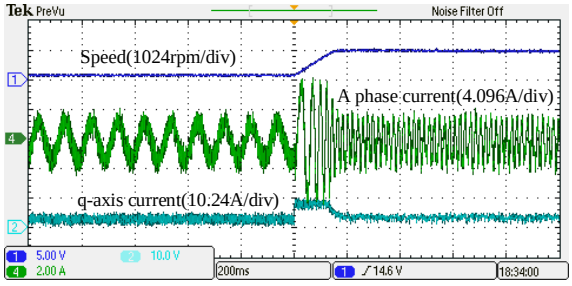

(a)

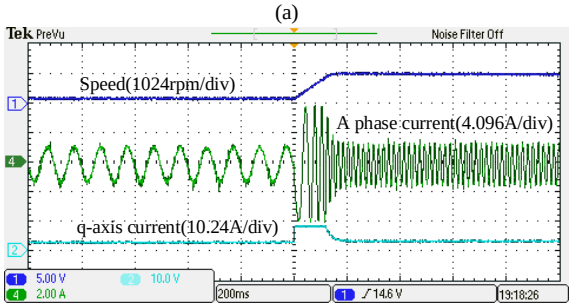

(b)

Fig. 14. Experimental results under target speed changing from 200*rpm* to 1000*rpm*. (a) SFCS-MPC. (b) OST-M2PC.

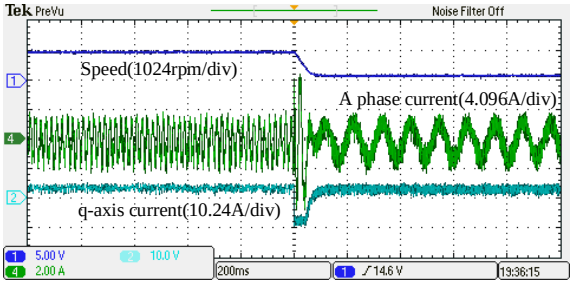

(a)

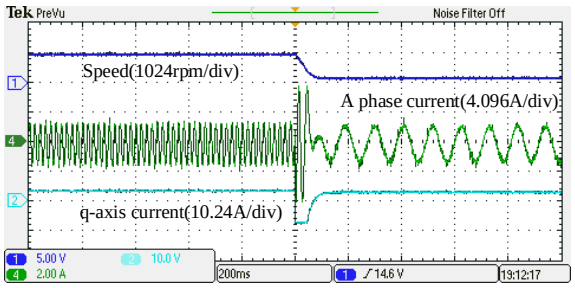

(b)

Fig. 15. Experimental results under speed changing from 1000*rpm* to 200*rpm*. (a) SFCS-MPC. (b) OST-M2PC.

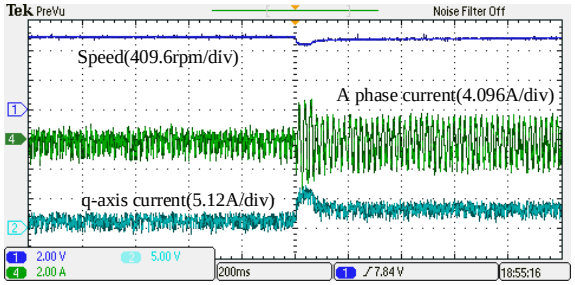

(a)

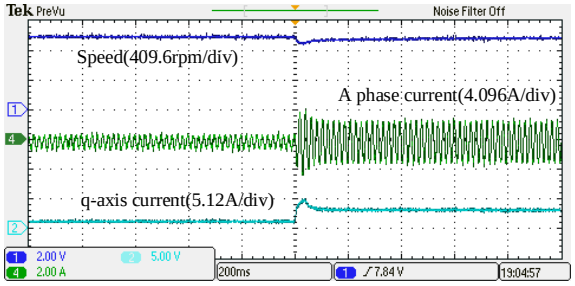

(b)

Fig. 16. Experimental results under sudden load disturbance at 1000*rpm*. (a) SFCS-MPC. (b) OST-M2PC.

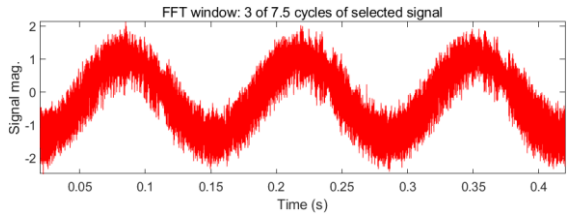

(a)

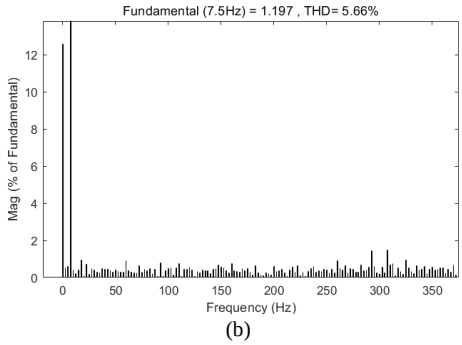

(b)

Fig. 17. The wave spectrum for SFCS-MPC (Experimental results). (a) A-phase current. (b) Harmonic spectrum of a-phase current.

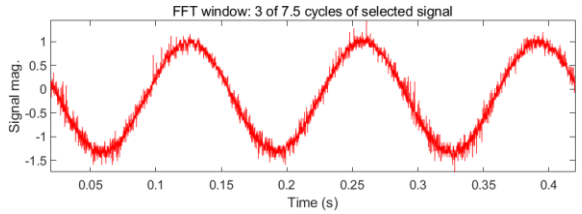

(a)

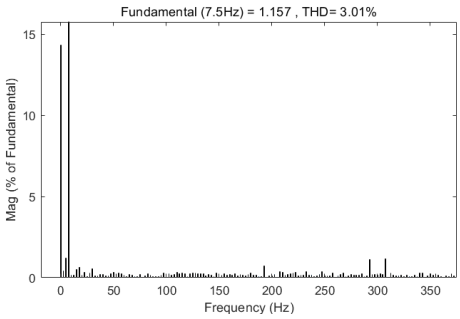

(b)

Fig. 18. The wave spectrum for OST-M2PC (Experimental results). (a) A-phase current. (b) Harmonic spectrum of a-phase current.

V. Conclusion

This paper presents a low-complexity optimal switching time modulated model predictive control (OST-M2PC) method for PMSM with three-level NPC converter. Different from the conventional FCS-MPC, the optimal switching time of OST-M2PC can be calculated by a cost function, which has a fixed switching frequency as well as better power quality. The proposed OST-M2PC method is easy to be implemented in a three-level NPC converter. The conventional FCS-MPC cannot run with a high sampling frequency because of computing limitation of the processor. To confirm the effects of OST-M2PC method and compare with the traditional FCS-MPC method at a high sampling frequency, a simplified finite control set model predictive control (SFCS-MPC) for a three-level NPC converter is proposed. The use of OST-M2PC shows reduced current ripple from simulation and experimental results. However, similar with other MPC methods, OST-M2PC is still a model-based approach. When the motor parameters are not accurate, the control performance will be affected. As for future works, the proposed OST-M2PC with an actual parameter disturbance observer such as luenberger [28], ESO [29], [30] or SMO [31] based approach will be used to improve robust ability of OST-M2PC.

References

[1] C. Xiong, H. Xu, T. Guan, and P. Zhou, "A Constant Switching Frequency Multiple-Vector-Based Model Predictive Current Control of Five-Phase PMSM With Nonsinusoidal Back EMF," *IEEE Trans. Ind. Electron.*, vol. 67, no. 3, pp. 1695–1707, Mar. 2020, doi: 10.1109/TIE.2019.2907502.

[2] Z. Wang, A. Yu, X. Li, G. Zhang, and C. Xia, "A Novel Current Predictive Control Based on Fuzzy Algorithm for PMSM," *IEEE J. Emerg. Sel. Top. Power Electron.*, vol. 7, no. 2, pp. 990–1001, Jun. 2019, doi: 10.1109/JESTPE.2019.2902634.

[3] C. Wang and Z. Q. Zhu, "Fuzzy Logic Speed Control of Permanent Magnet Synchronous Machine and Feedback Voltage Ripple Reduction in Flux-Weakening Operation Region," *IEEE Trans. Ind. Appl.*, vol. 56, no. 2, pp. 1505–1517, Mar. 2020, doi: 10.1109/TIA.2020.2967673.

[4] Z. Yin, L. Gong, C. Du, J. Liu, and Y. Zhong, "Integrated Position and Speed Loops Under Sliding-Mode Control Optimized by Differential Evolution Algorithm for PMSM Drives," *IEEE Trans. Power Electron.*, vol. 34, no. 9, pp. 8994–9005, Sep. 2019, doi: 10.1109/TPEL.2018.2889781.

[5] X. Yuan, S. Zhang, and C. Zhang, "Improved Model Predictive Current Control for SPMSM Drives With Parameter Mismatch," *IEEE Trans. Ind. Electron.*, vol. 67, no. 2, pp. 852–862, Feb. 2020, doi: 10.1109/TIE.2019.2901648.

[6] J. Rodriguez, S. Bernet, P. K. Steimer, and I. E. Lizama, "A Survey on Neutral-Point-Clamped Inverters," *IEEE Trans. Ind. Electron.*, vol. 57, no. 7, pp. 2219–2230, Jul. 2010, doi: 10.1109/TIE.2009.2032430.

[7] G. Liu, C. Song, and Q. Chen, "FCS-MPC-Based Fault-Tolerant Control of Five-Phase IPMSM for MTPA Operation," *IEEE Trans. Power Electron.*, vol. 35, no. 3, pp. 2882–2894, Mar. 2020, doi: 10.1109/TPEL.2019.2931712.

[8] M. R. Nasiri, S. Farhangi, and J. Rodriguez, "Model Predictive Control of a Multilevel CHB STATCOM in Wind Farm Application Using Diophantine Equations," *IEEE Trans. Ind. Electron.*, vol. 66, no. 2, pp. 1213–1223, Feb. 2019, doi: 10.1109/TIE.2018.2833055.

[9] M. Novak, U. M. Nyman, T. Dragicevic, and F. Blaabjerg, "Analytical Design and Performance Validation of Finite Set MPC Regulated Power Converters," *IEEE Trans. Ind. Electron.*, vol. 66, no. 3, pp. 2004–2014, Mar. 2019, doi: 10.1109/TIE.2018.2838073.

[10] Y. Luo and C. Liu, "Pre- and Post-Fault Tolerant Operation of a Six-Phase PMSM Motor Using FCS-MPC Without Controller Reconfiguration," *IEEE Trans. Veh. Technol.*, vol. 68, no. 1, pp. 254–263, Jan. 2019, doi: 10.1109/TVT.2018.2883665.

[11] C. Xia, T. Liu, T. Shi, and Z. Song, "A Simplified Finite-Control-Set Model-Predictive Control for Power Converters," *IEEE Trans. Ind. Inform.*, vol. 10, no. 2, pp. 991–1002, May 2014, doi: 10.1109/TII.2013.2284558.

[12] Y. Zhang, W. Xie, Z. Li, and Y. Zhang, "Model Predictive Direct Power Control of a PWM Rectifier With Duty Cycle Optimization," *IEEE Trans. Power Electron.*, vol. 28, no. 11, pp. 5343–5351, Nov. 2013, doi: 10.1109/TPEL.2013.2243846.

[13] L. Tarisciotti, P. Zanchetta, A. Watson, J. Clare, S. Bifaretti, and M. Rivera, "A new predictive control method for cascaded multilevel converters with intrinsic modulation scheme," in *IECON 2013 - 39th Annual Conference of the IEEE Industrial Electronics Society*, Nov. 2013, pp. 5764–5769, doi: 10.1109/IECON.2013.6700079.

[14] L. Tarisciotti, P. Zanchetta, A. Watson, S. Bifaretti, and J. C. Clare, "Modulated model predictive control for a seven-level cascaded h-bridge back-to-back converter," *IEEE Trans. Ind. Electron.*, vol. 61, no. 10, pp. 5375–5383, 2014, doi: 10.1109/TIE.2014.2300056.

[15] L. Tarisciotti *et al.*, "Modulated Predictive Control for Indirect Matrix Converter," *IEEE Trans. Ind. Appl.*, vol. 53, no. 5, pp. 4644–4654, Sep. 2017, doi: 10.1109/TIA.2017.2699666.

[16] M. Rivera *et al.*, "A modulated model predictive control scheme for a two-level voltage source inverter," in *2015 IEEE International Conference on Industrial Technology (ICIT)*, Mar. 2015, pp. 2224–2229, doi: 10.1109/ICIT.2015.7125425.

[17] M. Rivera *et al.*, "Modulated Model Predictive Control (M2PC) with fixed switching frequency for an NPC converter," in *2015 IEEE 5th International Conference on Power Engineering, Energy and Electrical Drives (POWERENG)*, Riga, Latvia, May 2015, pp. 623–628, doi: 10.1109/PowerEng.2015.7266389.

[18] F. Donoso, A. Mora, R. Cardenas, A. Angulo, D. Saez, and M. Rivera, "Finite-Set Model-Predictive Control Strategies for a 3L-NPC Inverter Operating With Fixed Switching Frequency," *IEEE Trans. Ind. Electron.*, vol. 65, no. 5, pp. 3954–3965, May 2018, doi: 10.1109/TIE.2017.2760840.

[19] S. Xie, Y. Sun, M. Su, J. Lin, and Q. Guang, "Optimal switching sequence model predictive control for three-phase Vienna rectifiers," *IET Electr. Power Appl.*, vol. 12, no. 7, pp. 1006–1013, 2018, doi: 10.1049/iet-epa.2018.0033.

[20] P. C. Krause, O. Wasynczuk, and S. D. Sudhoff, *Analysis of Electric Machinery*. New York: Wiley-IEEE Press, 1995.

[21] S. Li, M. Zhou, and X. Yu, "Design and Implementation of Terminal Sliding Mode Control Method for PMSM Speed Regulation System," *IEEE Trans. Ind. Inform.*, vol. 9, no. 4, pp. 1879–1891, Nov. 2013, doi: 10.1109/TII.2012.2226896.

[22] R. Vargas, P. Cortes, U. Ammann, J. Rodriguez, and J. Pontt, "Predictive Control of a Three-Phase Neutral-Point-Clamped Inverter," *IEEE Trans. Ind. Electron.*, vol. 54, no. 5, pp. 2697–2705, Oct. 2007, doi: 10.1109/TIE.2007.899854.

[23] Q. Wang, M. Rivera, J. A. Riveros, and P. Wheeler, "Modulated Model Predictive Current Control for PMSM Operating With Three-level NPC Inverter," in *2019 IEEE 15th Brazilian Power Electronics Conference and 5th IEEE Southern Power Electronics Conference (COBEP/SPEC)*, Dec. 2019, pp. 1–5, doi: 10.1109/COBEP/SPEC44138.2019.9065401.

[24] X. Li *et al.*, "A Modulated Model Predictive Control Scheme for the Brushless Doubly Fed Induction Machine," *IEEE J. Emerg. Sel. Top. Power Electron.*, vol. 6, no. 4, pp. 1681–1691, Dec. 2018, doi: 10.1109/JESTPE.2018.2865668.

[25] F. Donoso, A. Mora, R. Cardenas, A. Angulo, D. Saez, and M. Rivera, "Finite-Set Model-Predictive Control Strategies for a 3L-NPC Inverter Operating With Fixed Switching Frequency," *IEEE Trans. Ind. Electron.*, vol. 65, no. 5, pp. 3954–3965, May 2018, doi: 10.1109/TIE.2017.2760840.

[26] L. Tarisciotti, P. Zanchetta, A. Watson, J. C. Clare, M. Degano, and S. Bifaretti, "Modulated Model Predictive Control for a Three-Phase Active Rectifier," *IEEE Trans. Ind. Appl.*, vol. 51, no. 2, pp. 1610–1620, Mar. 2015, doi: 10.1109/TIA.2014.2339397.

[27] S.-W. Kang, J.-H. Soh, and R.-Y. Kim, "Symmetrical Three-Vector-Based Model Predictive Control With Deadbeat Solution for IPMSM in Rotating Reference Frame," *IEEE Trans. Ind. Electron.*, vol. 67, no. 1, pp. 159–168, Jan. 2020, doi: 10.1109/TIE.2018.2890490.

[28] C. Xia, M. Wang, Z. Song, and T. Liu, "Robust Model Predictive Current Control of Three-Phase Voltage Source PWM Rectifier With Online Disturbance Observation," *IEEE Trans. Ind. Inform.*, vol. 8, no. 3, pp. 459–471, Aug. 2012, doi: 10.1109/TII.2012.2187912.

[29] L. Qu, W. Qiao, and L. Qu, "An Extended-State-Observer-Based Sliding-Mode Speed Control for Permanent-Magnet Synchronous Motors," *IEEE J. Emerg. Sel. Top. Power Electron.*, pp. 1–1, 2020, doi: 10.1109/JESTPE.2020.2990442.

[30] H. Liu and S. Li, "Speed Control for PMSM Servo System Using Predictive Functional Control and Extended State Observer," *IEEE Trans. Ind. Electron.*, vol. 59, no. 2, pp. 1171–1183, Feb. 2012, doi: 10.1109/TIE.2011.2162217.

[31] X. Zhang, B. Hou, and Y. Mei, "Deadbeat Predictive Current Control of Permanent-Magnet Synchronous Motors with Stator Current and Disturbance Observer," *IEEE Trans. Power Electron.*, vol. 32, no. 5, pp. 3818–3834, May 2017, doi: 10.1109/TPEL.2016.2592534.

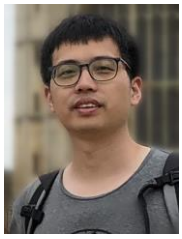

Qi Wang (S'18) received the B.Sc. degree from the PLA Information Engineering University, Zhengzhou, China, in 2008, and the M.Sc. degree from Guangxi University, Nanning, China, in 2011. He is currently working toward the Ph.D. degree in electrical engineering at Southeast University, Nanjing, China. From July 2011 to September 2012, he was an Assistant Engineer in State Grid Electric Power Research Institute, Nanjing, China. From January 2019 to January 2020, he got the scholarship from China Scholarship Council and was a joint Ph.D. Student with the Power Electronics, Machines and Control (PEMC) Research Group, School of Electrical and Electronic Engineering, University of Nottingham, Nottingham, U.K. His research interests include model predictive control, sliding mode control, AC motor drives, and power electronic coverters.

Haitao Yu received the B.Sc. and M.Sc. degree in electric engineering from Chongqing University, Chongqing, China, in 1986 and 1989, respectively, and the Ph.D. degree in electric engineering from Huazhong University of Science and Technology, Wuhan, China, in 1995. He was an Associate Professor at the Huazhong University of Science and Technology in 1997. From 1998 to 2002, he was a Research Fellow at Duke University, Durham, NC, USA. He is currently a Professor in the school of Electrical Engineering at Southeast University, Nanjing, China. His main research interests include new energy power generation, electric vehicle, and motor drives.

Chen Li (S'18) received the B.Sc. degree in electrical and electronics engineering from the University of Nottingham, Nottingham, U.K., in 2016. He is currently working toward the Ph.D degree with the Power Electronics, Machines and Control Group, University of Nottingham, Nottingham, U.K. His research interests include high-speed drives, aerospace power electronic converters, more electric aircraft, and sensorless control of ac drives.

Xiaoyu Lang (S'19) received the B.S. degree and M.Sc. degree (Honors) in electrical engineering from the Harbin Institute of Technology (HIT), Harbin, China, in 2015 and 2017, respectively. He is currently working toward the Ph.D degree with the Power Electronics, Machines and Control Group, University of Nottingham, Nottingham, U.K. His research interests include high speed machine drives, advanced integrated power generation centre for more electric aircrafts, and DC microgrid stability.

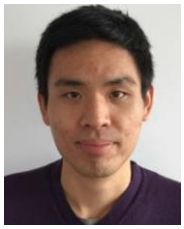

Seang Shen Yeoh received the M.Sc. degree in power electronics and drives and the Ph.D. degree in electrical engineering from the University of Nottingham, Nottingham, U.K., in 2011 and 2016, respectively. Since 2016, he has been a Research Fellow with the Power Electronics, Machines, and Control (PEMC) Research Group, University of Nottingham. His current research interests include modeling and stability studies of complex power systems, and control strategies for power electronic drive systems.

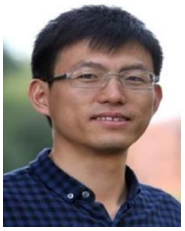

Tao Yang (M'16) received the Ph.D. degree in electrical engineering from the University of Nottingham, Nottingham, U.K., in 2013. He is currently an Associate Professor with the Power Electronics, Machines and Control Group, University of Nottingham. His research interests include aircraft electrical power systems and high-speed motor drives for aerospace applications.

Marco Rivera (S'09–M'11–SM'17) received the B.Sc. degree in electronics engineering and the M.Sc. degree in electrical engineering from the Universidad de Concepci´on, Concepci´on, Chile, in 2007 and 2008, respectively, and the Ph.D. degree in electronics engineering from Universidad T´ecnica Federico Santa Mar´ıa, Valpara´ıso, Chile, in 2011, with a scholarship from the Chilean Research Fund CONICYT. During 2011 and 2012, he was a Postdoctoral Researcher and part-time Professor with the Department of Electronics Engineering, Universidad T´ecnica Federico Santa Mar´ıa. He is currently a Professor with the Department of Electrical Engineering, Universidad de Talca, Curic ´ o, Chile. His research interests include matrix converters, predictive and digital controls for high-power drives, four-leg converters, and the development of highperformance control platforms based on field-programmable gate arrays.

Serhiy Bozhko (M'96–SM'18) received the M.Sc. (Hons.) and Ph.D. degrees in electromechanical systems from the National Technical University of Ukraine, Kyiv, Ukraine, in 1987 and 1994, respectively. Since 2000, he has been with the Power Electronics, Machines and Control (PEMC) Research Group, University of Nottingham, Nottingham, U.K., where he is currently a Professor leading several Euand industry-funded projects in the area of aircraft electric power systems, including control, power quality and stability issues, power management and optimization, as well as advanced modeling and simulations methods.

Pat Wheeler (M'94–SM'08) received the B.Sc. (Hons.) and the Ph.D. degrees in electrical engineering from the University of Bristol, Bristol, U.K., in 1990 and 1994, respectively. In 1993, he moved to the University of Nottingham and worked as a Research Assistant with the Department of Electrical and Electronic Engineering. In 1996, he became a Lecturer with the Power Electronics, Machines and Control Group, University of Nottingham, where he has been a Full Professor since January 2008. He was the Head of the Department of Electrical and Electronic Engineering, University of Nottingham from 2015 to 2018. He is currently the Head of the Power Electronics, Machines and Control Research Group and is the Li Dak Sum Chair Professor in electrical and aerospace engineering with the University of Nottingham Ningbo China, Ningbo, China. He has published 500 academic publications in leading international conferences and journals. Dr. Wheeler is a member of the IEEE PELs AdCom and was an IEEE PELs Distinguished Lecturer from 2013 to 2017.